J Physiol (2003), **548.1**, *pp.* 245–258
DOI: 10.1113/jphysiol.2002.036376

www.jphysiol.org

Journal of Physiology

Mechanism of the distance-dependent scaling of Schaffer collateral synapses in rat CA1 pyramidal neurons

Mark A. Smith, Graham C. R. Ellis-Davies* and Jeffrey C. Magee

*Neuroscience Center, LSUHSC, 2020 Gravier Street, New Orleans, LA 70112 and *Department of Pharmacology and Physiology, Drexel University College of Medicine, Philadelphia, PA 19102, USA*

Schaffer collateral axons form excitatory synapses that are distributed across much of the dendritic arborization of hippocampal CA1 pyramidal neurons. Remarkably, AMPA-receptor-mediated miniature EPSP amplitudes at the soma are relatively independent of synapse location, despite widely different degrees of dendritic filtering. A progressive increase with distance in synaptic conductance is thought to produce this amplitude normalization. In this study we examined the mechanism(s) responsible for spatial scaling by making whole-cell recordings from the apical dendrites of CA1 pyramidal neurons. We found no evidence to suggest that there is any location dependence to the range of cleft glutamate concentrations found at Schaffer collateral synapses. Furthermore, we observed that release probability (P_r), paired-pulse facilitation and the size of the readily releasable vesicular pool are not dependent on synapse location. Thus, there do not appear to be any changes in the fundamental presynaptic properties of Schaffer collateral synapses that could account for distance-dependent scaling. On the other hand, two-photon uncaging of 4-methoxy-7-nitroindolinyl-caged L-glutamate onto isolated dendritic spines shows that the number of postsynaptic AMPA receptors per spine increases with distance from the soma. We conclude, therefore, that the main synaptic mechanism involved in the production of distance-dependent scaling of Schaffer collateral synapses is an elevated postsynaptic AMPA receptor density.

(Received 22 November 2002; accepted after revision 21 January 2003; first published online 21 February 2003)
Corresponding author M. A. Smith: Neuroscience Center, LSUHSC, 2020, Gravier Street, New Orleans, LA 70112, USA.
Email: msmith19@lsuhsc.edu

Schaffer collateral axons originating from CA3 pyramidal neurons form spiny, excitatory glutamatergic synapses on the dendritic arborization of CA1 pyramidal neurons located within the stratum radiatum. This pathway provides the numerically largest excitatory synaptic input received by the CA1 pyramidal neuron.

It is widely recognized that the filtering properties of dendrites shape the amplitude and width of excitatory postsynaptic potentials (EPSPs) to a degree that is dependent upon synapse location (Rall, 1962; Jack & Redman, 1971; Jaffe & Carnevale, 1999). However, in CA1 pyramidal neurons it has been demonstrated that the unitary EPSP amplitude increases with distance from the soma, helping to compensate for the filtering effects of the dendrite (Stricker *et al.* 1996; Magee & Cook, 2000). Due to this compensatory mechanism, Schaffer collateral axons can form synapses at varying locations along the CA1 pyramidal dendrite, but maintain a functionally homogeneous somatic input. The mechanisms underlying EPSP scaling appear to involve a progressive increase in the AMPA-receptor-mediated synaptic conductance (Magee & Cook, 2000; Andrásfalvy & Magee, 2001). Although no such scaling mechanism has been reported in neocortical layer V pyramidal neurons (Williams & Stuart, 2002), spatial scaling of synaptic conductance has been observed in other CNS preparations (Insasek & Redman, 1973; Korn *et al.* 1993; Alvarez *et al.* 1997).

In light of these findings, we have examined the location dependence of various fundamental synaptic properties of Schaffer collateral input onto CA1 pyramidal neurons. Data presented in this paper indicate that cleft transmitter concentration, the immediate releasable pool size and the probability of release (P_r) do not differ between proximal and distal locations. However, the mechanism of synaptic scaling in these neurons appears to be due to a progressive increase in the postsynaptic AMPA receptor density.

METHODS

Hippocampal slices were made from 6- to 12-week-old Sprague-Dawley rats as described previously (Magee, 1998). According to methods approved by the LSUHSC Institutional Animal Care and Use Committee, rats were given a lethal dose of ketamine and xylazine, perfused through the ascending aorta with a 95% O_2–5% CO_2 bubbled solution just before death, and then decapitated. Individual neurons were visualized with a Zeiss Axioskop microscope (Oberkochen, Germany) fitted with differential interference contrast optics using infrared illumination.

Whole-cell voltage-clamp recordings were made at −70 mV using an Axopatch 200B amplifier (Axon Instruments, Foster City, CA, USA). Currents were filtered at 5 kHz and captured at 50 kHz using Igor Pro (WaveMetrics, Lake Oswego, OR, USA). The standard external solution contained (mM): 125 NaCl, 2.5 KCl, 1.25 NaH_2PO_4, 25 $NaHCO_3$, 2 $CaCl_2$, 1 $MgCl_2$ and 25 D-glucose, aspirated with 95 % O_2 and 5 % CO_2 (pH 7.4). In general, recordings were made at ~33 °C, although uncaging experiments were performed at ~30 °C. AMPA currents were recorded in the presence of external DL-aminophosphonovalerate (APV, 50 μM) and (+)-bicuculline (10 μM). In experiments where NMDA currents were recorded, $MgCl_2$ was replaced with $CaCl_2$ (2.5 mM final concentration) and APV was replaced with 1,2,3,4-tetrahydro-6-nitro-2,3-dioxo-benzo[f]quinoxaline-7-sulphonamide (NBQX, 5 μM). Recording electrodes were pulled from borosilicate glass and had resistances of 4–8 MΩ when filled with internal solution containing (mM): 120 Cs-gluconate, 20 $CsCl_2$, 0.5 EGTA, 4 NaCl, 0.3 $CaCl_2$, 4 Mg_2ATP, 0.3 $Tris_2GTP$, 14 phosphocreatine and 10 Hepes (pH 7.2). In addition, QX-314 (5 mM; a non-selective Na^+ channel inhibitor) was added to the internal solution for experiments studying NMDA currents and the immediate releasable pool size. Series resistances from dendritic whole-cell recordings were between 10 and 30 MΩ.

Single miniature synaptic events (mEPSCs) were evoked by pressure ejection of a hyperosmotic external solution (+300 mM sucrose), tetrodotoxin (TTX, 0.5 μM) and Hepes (10 mM) replacing $NaHCO_3$ (~700 mosmol l^{-1}; Magee & Cook, 2000). In addition, TTX (0.5 μM) was added to the bathing solution. In the majority of experiments, the external solution was ejected from separate barrels of a borosilicate theta tube pulled to a tip diameter of ~2 μm. One side of the theta tube contained a control (high osmolarity) external solution, whereas the other side had a solution containing kynurenic acid (200 μM), GYKI-52466 (15 μM) or cyclothiazide (CTZ, 400 μM). An alternative method of obtaining unitary events was to replace external Ca^{2+} with Sr^{2+} (8 mM, in the absence of TTX) and stimulate electrically with a 0.1 mm tungsten bipolar electrode (A-M systems, Carlsberg, WA, USA) located ~20 μm adjacent to the dendrite.

mEPSCs were analysed for peak amplitude, and rise and decay time constants (sum of two exponential functions) using a template fit algorithm written in Igor Pro (Magee & Cook, 2000). Events were collected between 1 and 7 s following pressure ejection of high-osmolarity solutions and between 40 ms and 1 s following stimulation in Sr^{2+}. Only events crossing a 3 pA threshold level were examined further. In general, events that had rise-time constants greater than 400 μs were eliminated from analysis, since these events were unlikely to be local (Magee & Cook, 2000). However, in experiments measuring the properties of dendritic filtering and CTZ, no rise-time constant threshold was assigned. Cumulative frequency histograms were constructed from between 50 and 200 unitary events per condition.

For MNI (4-methoxy-7-nitroindolinyl)–glutamate (MNI-glu)-uncaging experiments, hippocampal CA1 pyramidal neurons were visualized using an upright Olympus BX50WI microscope (Olympus America, Melville, NY, USA) fitted with a × 100, 1.0 NA water-immersion objective lens. A mode-locked, femtosecond-pulse Ti:sapphire laser (Coherent, Auburn, CA, USA) was scanned with a modified confocal scan head (FluoView, Olympus America) and gated with a mechanical shutter at 2–4 ms (Uniblitz, Rochester, NY, USA). The point spread function of focal volume for two-photon excitation (Fig. 9*D* and *G*), estimated using 0.1 μm fluorescent beads, was 0.34 μm laterally and 1.4 μm axially (full width, half maximum; FWHM). The FWHM of glutamate current amplitude distributions obtained by point uncaging of MNI-glu (720 nm, 5 mW) at different locations (~0.16 μm lateral and 0.5 μm axial steps) on well-isolated spines was 0.6 μm laterally and 2.0 μm axially (Fig. 9). That the uncaging volume is larger than the focal volume indicates that this measurement is a combination of the point release resolution and some glutamate diffusion (Matsuzaki *et al.* 2001). However, the concentration of glutamate following release is only sufficiently high to activate AMPA receptors within the coordinates defined by the uncaging resolution (Fig. 9). Therefore, isolated spines were identified on the basis that no other spine was within 1 μm of the examined spine in the same lateral plane and no other spine was directly below or above this perimeter (as determined by *z*-stack reconstruction, Fig. 9*A* and *B*). For spines showing a head diameter greater than 0.4 μm, head volume was estimated directly from the spine head diameter determined from fluorescence point spread functions (FWHM) and substituted in the equation for a sphere:

$$\text{Volume} = 4/3\pi r^3,$$

where r is the spine head radius. For spines with a smaller diameter, volume was estimated by referencing the total fluorescence of the spine head acquired from three-dimensional reconstructions to the total fluorescence of a large (> 0.4 μm) spine head whose volume could be estimated as above (Matsuzaki *et al.* 2001).

For uncaging experiments, hippocampal slices were incubated in the standard external solution in the presence of TTX (0.5 μM), APV (50 μM) and ascorbate (2 mM). Whole-cell dendritic recordings were made using patch pipettes containing a Ca^{2+}-free standard caesium gluconate solution in the presence of ascorbate (2 mM) and bis-Fura (150 μM; Molecular Probes, Eugene, OR, USA) replacing EGTA. Dendrites were voltage-clamped at −70 mV using an Axopatch 1D amplifier (Axon Instruments) and had access resistances of 15–30 MΩ. In addition, a broken pipette containing the standard external solution in the presence of TTX (0.5 μM), APV (50 μM), ascorbate (2 mM), CTZ (100 μM) and caged MNI-glu (12 mM) was positioned above the slice at the site of the recording electrode. Measurement of the fluorescence profile of Alexa 594 hydrizide (0.2 mM) applied in a similar manner suggested that concentrations were constant for up to 25 μm below the surface of the slice. Thus all spines used were between 15 and 20 μm below the surface of the slice. The potential for errors resulting from daily fluctuations in laser power or cage compound efficacy was controlled for by the acquisition of both proximal and distal spine data within the same day. Furthermore, the data-collection period was limited to approximately 15 min per cell in order to reduce the chance of phototoxicity and desensitization (even though CTZ was present).

The microscopic properties of AMPA channels were examined using non-stationary fluctuation analysis (Sigworth, 1980). AMPA currents were evoked every 5 s (5 mW, 2 ms shutter speed) and 15–40 traces were obtained per spine. The mean current was plotted against individual trace variance (initial 10–25 ms) and fitted with the following equation:

$$\sigma^2 = iI - (1/N)I^2 + \sigma_b^2,$$

where I is the total current, i is the single channel current, N is the number of available channels, and σ_b^2 is the variance of the

background noise. Channel open probability (P_o) was determined from:

$$P_o = I/(i/N).$$

Reagents were obtained from Sigma (St Louis, MO, USA), except APV, QX-314 and MK801, which were purchased from Tocris Cookson (Ballwin, MO, USA), and TTX, which was acquired from Alomone Labs (Jerusalem, Israel). MNI-glu was synthesized as described previously (Matsuzaki *et al.* 2001). Unless stated otherwise, all data are expressed as means ± S.E.M. Statistical significance was determined at the 5% level of confidence using Student's *t* test and linear regression.

RESULTS

Whole-cell voltage-clamp recordings were made from the apical dendrites of hippocampal CA1 pyramidal neurons. In this study, proximal (100–140 μm) and distal (240–280 μm) locations correspond to the spiny region of the stratum radiatum that is almost exclusively innervated by excitatory Schaffer collateral axons (Megías *et al.* 2001). mEPSCs were evoked by localized application of a high-osmolarity external solution. Consistent with previous findings, AMPA-receptor-mediated mEPSC amplitudes were quite variable in all locations (coefficient of variation: proximal 0.69 ± 0.10; distal 0.75 ± 0.02; Magee & Cook, 2000), with the mean amplitudes for events recorded from proximal and distal locations being 11.0 ± 1.1 ($n = 15$) and 26.8 ± 2.0 pA ($n = 26$, $P < 10^{-6}$), respectively (Fig. 1*A*). The difference in amplitude between proximal and distal events was clearly indicated by a fairly uniform shift of distal events in the cumulative amplitude distribution (Fig. 1*B* and *C*) to larger amplitudes.

It can be argued that the smaller-amplitude proximal mEPSCs are actually distant events that have been filtered more by the passive properties of the dendrite than the larger, more distal events. However, as dendritic filtering is frequency dependent, the rise-time kinetics of highly filtered mEPSCs should be dramatically slower than lesser-filtered events. This was demonstrated by recording at one dendritic location and focally applying a high-osmolarity solution at both the site of the recording electrode and a second, more distant site of the same dendrite (~80 μm either more proximal or distal). The mean rise-time constant of mEPSCs evoked at the site of the recording electrode was 189 ± 34 μs, which contrasts with 324 ± 21 μs ($n = 6$, $P < 0.03$) for events evoked at the more distant location (Fig. 2*A* and *D*). The slowing of rise times by dendritic filtering was best demonstrated by the cumulative frequency distribution (Fig. 2*B* and *E*), which showed a clear shift to slower time constants for events evoked at the distant compared to the local region. Mean mEPSC decay time constants (local 4.1 ± 0.3 ms, distant 4.8 ± 0.8 ms) were not significantly different between the two synaptic populations ($P > 0.5$), and only the amplitudes of events evoked more proximal to the recording site were smaller (proximal recording site: locally evoked 12.8 ± 2.1 pA, distally evoked 15.0 ± 4.9 pA, Fig. 2*C*; distal recording site: locally evoked 22.6 ± 3.2 pA, proximally evoked 14.7 ± 2.4 pA, Fig. 2*D*; $P < 0.05$). These data clearly show that events generated some distance away from the recording pipette (~80 μm) exhibit extremely filtered rise times. As no such differences were observed between the rise-time kinetics of distal and proximal mEPSCs (proximal 169 ± 10 μs, $n = 15$; distal 184 ± 6 μs, $n = 26$; $P > 0.2$), we conclude that the vast majority of all recorded events (both proximal and distal)

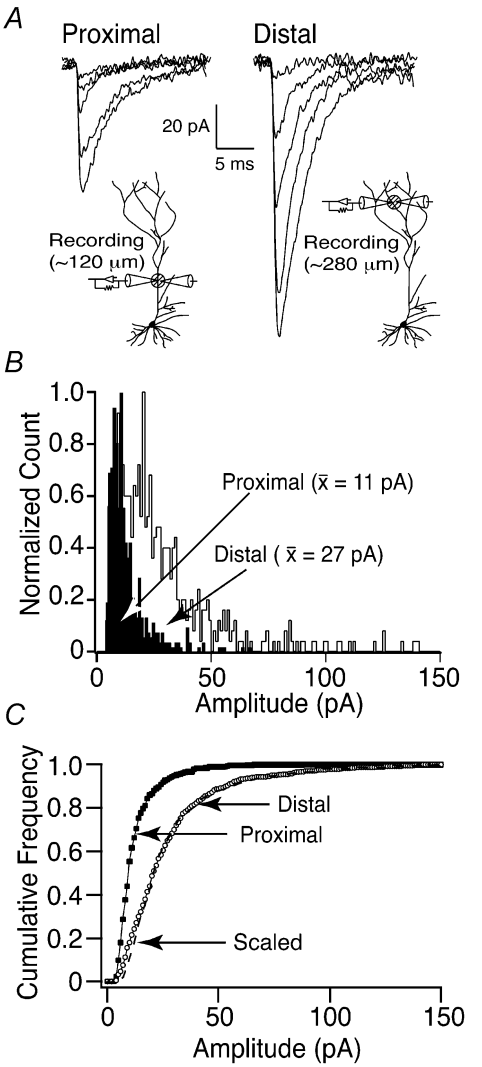

Figure 1. AMPA-mediated miniature EPSC (mEPSC) amplitudes are spatially scaled

A, superimposed representative current traces of mEPSCs evoked by high osmolarity for proximal (left, ~120 μm) and distal (right, ~280 μm) dendritic regions. *B*, normalized frequency histograms of proximal and distal mEPSC amplitudes. Mean amplitudes are shown in parentheses for proximal ($n = 15$) and distal synapses ($n = 26$). *C*, normalized cumulative frequency distributions for proximal (■) and distal (○) mEPSC amplitudes. The dashed line shows a scaled (× 2.5) proximal cumulative distribution. Note the level of overlap between the scaled proximal and the distal distributions.

were produced by synapses located equally close to the recording electrode (possibly within 25 μm).

We examined further the kinetic properties of dendritic mEPSCs and found a significant positive correlation between mEPSC amplitudes and the rise-time constants of both proximal and distal (Fig. 3*A* and *B*, respectively) synapses, although the slope differed significantly ($P < 0.0004$), with values of 6.9 ± 1.1 μs pA^{-1} ($n = 15$) and 2.4 ± 0.5 μs pA^{-1} ($n = 26$), respectively. The slopes of the relationships are different because the range of mEPSC amplitudes, but not rise-time constants, is so much larger in the distal group of synapses compared with proximal. This is easily observed in plots where mEPSC amplitude has been normalized. In this case, plots of normalized amplitude against rise times for proximal and distal locations almost overlap (Fig. 3*C*).

Unlike rise times, mEPSC decay time constants for proximal and distal synapses showed no correlation with amplitude under control conditions (Fig. 3*D* and *E*, respectively). It is likely that the proximal events decay more slowly (5.9 ± 0.2 ms, $n = 15$ *versus* 4.4 ± 0.3 ms, $n = 26$; $P < 0.0002$) due to location-dependent differences in current flow in an imperfectly clamped neuron (Rall, 1967; Magee, 2000; Magee & Cook, 2000). However, as the decay kinetics of mEPSCs are shaped dramatically by AMPA-receptor desensitization (Vyklicky *et al.* 1991; Trussel *et al.* 1993), events were also evoked in the presence of cyclothiazide (~100 μM, CTZ), which abolishes desensitization (Diamond & Jahr, 1995; Rammes *et al.* 1998). Consistent with previous observations (Diamond & Jahr, 1995), CTZ slowed the mEPSC decay rate from 5.2 ± 0.4 to 8.0 ± 0.6 ms ($n = 5$, $P < 0.002$) for proximal (Fig. 4*A* and *B*) and from 3.5 ± 0.2 to 8.3 ± 0.5 ms ($n = 5$, $P < 0.003$) for distal events (Fig. 4*A* and *C*). However, mean mEPSC amplitude was unchanged for proximal (13.5 ± 2.3 for control to 14.1 ± 2.3 pA in CTZ) and for distal (28.0 ± 4.6 for control to 30.7 ± 6.2 pA in CTZ) events. In addition, no significant differences in rise-time constants were observed (proximal, 198 ± 25 for control

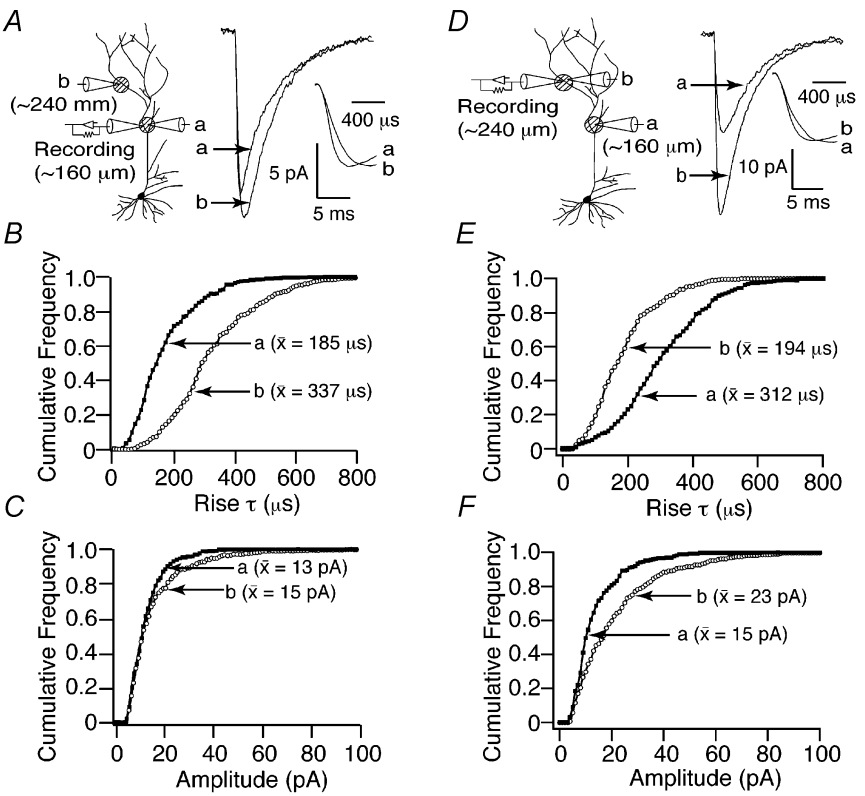

Figure 2. Effects of dendritic filtering on mEPSC kinetics

A, *B* and *C*, data from recordings made at a proximal dendritic location (~160 μm from the soma); unitary events were osmolarity-evoked at the site of the recording and at a more distal (~240 μm) location along the dendrite. *D*, *E* and *F*, distal recordings (~240 μm from soma) where unitary events were evoked at the site of the recording and at a more proximal (~160 μm) dendritic location. Representative mean current traces of mEPSCs are shown in panels *A* and *D* from proximal ('a') and distal ('b') dendritic locations. The faster rise-time constant of the locally evoked mean mEPSC is shown clearly in the insets on an expanded time scale, where currents are normalized to peak amplitude. *B* and *E*, normalized cumulative frequency histograms of mEPSC rise-time constants for proximal ('a') and distal ('b') events. Normalized cumulative frequency distributions of mEPSC amplitudes are shown in *C* and *F* for proximal ('a') and distal ('b') events. Mean mEPSC rise-time constants (*B* and *E*) and amplitudes (*C* and *F*) are shown in parentheses ($n = 3$).

and 200 ± 14 μs in CTZ; distal, 194 ± 19 for control and 233 ± 11 μs in CTZ). However, the most striking observation was that in the absence of AMPA-receptor desensitization, a positive correlation was found between mEPSC decay time constants and amplitude. This was observed for both proximal (Fig. 4*B*) and distal (Fig. 4*C*) events, although the slope again significantly differed ($P < 0.05$), with values of 0.17 ± 0.02 and 0.08 ± 0.04 ms pA^{-1}, respectively. However, as with rise-time constants, normalization of mEPSC amplitude removed the differences in the slopes of the amplitude *versus* decay time plots (Fig. 4*D*).

Monte Carlo synaptic simulations indicate that increasing the concentration of glutamate released in the absence of receptor desensitization generates currents that are larger in amplitude and have slower rise and decay time constants (Glavinovic & Rabie, 1998). Therefore, the wide-ranging variations of mEPSC kinetics observed in this and other studies could, in part, reflect fluctuations in cleft glutamate concentration. That mEPSC kinetic *versus* normalized amplitude plots showed no location-dependent differences suggests that regional changes in cleft glutamate are unlikely to underlie the distance-dependent scaling.

To determine further whether regional differences in cleft glutamate concentration exist, we compared the effect of fast-dissociating competitive glutamate-receptor antagonists on distal and proximal mEPSCs (Liu *et al.* 1999; Choi *et al.* 2000). The concept is based upon the reasonable assumption that higher concentrations of cleft glutamate will replace a weak, fast-dissociating antagonist more efficiently (Clements *et al.* 1992). Hyperosmotic-

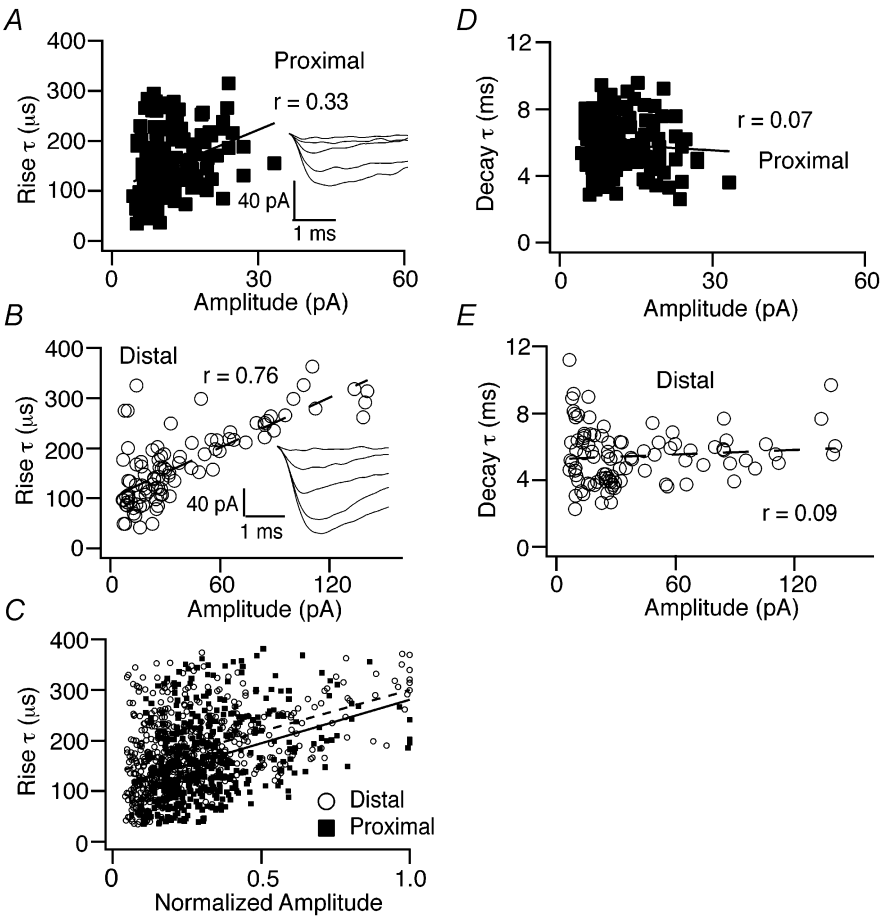

Figure 3. Kinetic properties of AMPA mEPSCs

Unitary synaptic events, evoked locally with a high-osmolarity solution, were recorded at proximal and distal regions. Representative plots of mEPSC amplitude against rise-time constants for proximal (■) and distal (○) synapses are shown in *A* and *B*, respectively. Plots are fitted with a linear regression, revealing significant correlations ($P < 0.05$). The insets in *A* and *B* show superimposed representative current traces of mEPSCs at proximal and distal locations, respectively. *C*, plot of mEPSC amplitude normalized to the peak amplitude of each cell ($n = 5$) against the rise-time constant for proximal (■) and distal (○) synapses. Note that the correlations fitted with a linear regression are almost superimposed for proximal and distal events. *D* and *E*, representative plots of mEPSC amplitude against decay time constants for proximal (■) and distal (○) synapses, respectively. Plots were fitted with a linear regression, and were found to display no significant correlation ($P > 0.05$).

evoked synaptic events were collected for the control condition and in the presence of bath-applied kynurenic acid (200 μM). In addition, kynurenic acid was added to one of the barrels of a theta tube. The mean amplitudes of proximal and distal (Fig. 5*A* and *C*, respectively) mEPSCs were reduced in the presence of kynurenic acid by 30 ± 5 ($n = 10$, $P < 0.004$) and 42 ± 7 % ($n = 15$, $P < 0.02$) of control, respectively. The non-competitive AMPA-receptor antagonist GYKI 52466 (15 μM) antagonized osmolarity evoked proximal and distal mEPSC mean amplitudes by 30 ± 5 ($n = 5$) and 45 ± 4 % ($n = 5$), respectively. These values are almost identical to the antagonism obtained using kynurenic acid, indicating that the slight differences in mean antagonism is a reflection of the loss of a larger fraction of the smaller proximal events into the recording noise, and was thus omitted from the analysis.

A plot of control amplitudes against the ratio between amplitudes at equal cumulative frequencies in the presence and absence of drug (I_d/I_c) revealed that kynurenic acid equally antagonized all synaptic amplitudes (Fig. 5*B* and *D*), regardless of synaptic location ($P > 0.08$). Moreover, mEPSC rise and decay time constants in the presence of kynurenic acid were not significantly different from controls for both proximal (rise: 168 ± 14 μs for control and 158 ± 10 μs in kynurenic acid; decay: 6.2 ± 0.2 ms for control and 6.0 ± 0.3 ms ($n = 10$) in kynurenic acid), and distal (rise: 184 ± 13 μs for control and 163 ± 11 μs in kynurenic acid; decay: 4.9 ± 0.5 ms for control and 5.3 ± 0.5 ms ($n = 15$) in kynurenic acid) events.

An alternative method used to obtain unitary events was electrical stimulation in Sr^{2+} (8 mM), which has been shown to desynchronize transmitter release (Bekkers & Clements, 1999; Fig. 6*A*). Consistent with the hyperosmotic experiments, kynurenic acid (200 μM) reduced the mean amplitude for distal synapses by 33 ± 6 % ($n = 10$, $P < 0.002$). In addition, plotting the control amplitude against the I_d/I_c ratio revealed that kynurenic acid equally antagonized all synaptic amplitudes (Fig. 6*B*). Furthermore, γ-D-glutamylglycine (γ-DGG, 1 mM; Fig. 6*C*) and the slower dissociating antagonist 6-cyano-7-nitroquinoxaline-2,3-dione (CNQX, 500 nM; Fig. 6*D*) also linearly antagonized Sr^{2+}-evoked distal synaptic currents by 38 ± 4 % ($n = 9, P < 0.005$) and 37 ± 5 % ($n = 9, P < 0.001$), respectively.

We next wanted to examine the possibility that larger synapses are responsible for the larger-amplitude events

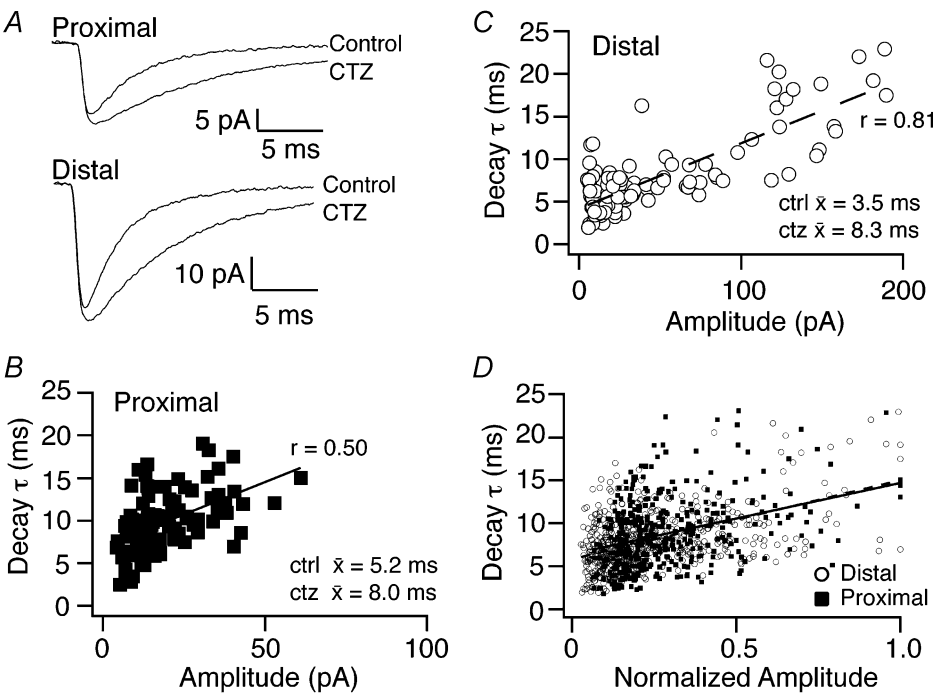

Figure 4. AMPA mEPSC decay time constants are correlated with amplitude in the absence of desensitization

A, representative ensemble mean current traces of osmolarity-evoked mEPSCs are shown, as indicated, in the absence and presence of cyclothiazide (CTZ, ~100 μM) for proximal (top) and distal (bottom) synapses. Note that the small increase in amplitude induced by CTZ in these cells is not reflected in the mean amplitude from multiple cells ($n = 5$). Representative plots of mEPSC amplitude against decay time constants in the presence of CTZ are shown for proximal (*B*) and distal (*C*) synapses. Plots were fitted with a linear regression ($P < 0.05$). *D*, plot of normalized mEPSC amplitude against decay time constant for proximal (■) and distal (○) synapses. Note that the correlations fitted with linear regression overlap for normalized proximal and distal events.

recorded from distal synapses. Larger synapses show larger active zones, docked releasable pool sizes, higher probabilities of release and larger event amplitudes (Schikorski & Stevens, 1999, 2001). If synapse size increases with distance from the soma, the size of the immediately releasable transmitter pool and the transmitter P_r should both be on average larger at distal compared to proximal synapses.

One method of measuring the immediate releasable pool size is to electrically evoke synaptic release in trains of stimuli and calculate number of stimuli required to deplete the releasable pool (Dobrunz & Stevens, 1997; Hagler & Goda, 2001). Using this method, we delivered trains of stimuli from a stimulating electrode located ~20 μm parallel to the recording electrode at a frequency of 20 Hz. In high P_r conditions, (4 mM external Ca^{2+}; 100 μM 4-aminopyridine (4-AP); 2 μM 1,3-dipropyl-8-cyclopentylxanthine (DPCPX), an adenosine A1-receptor antagonist) both proximal ($n = 7$) and distal ($n = 5$) EPSC amplitudes increased to a peak within three stimuli (Fig. 7*A* and *B*) and then proceeded to decay with further stimuli in a single exponential fashion (23.4 ± 7.8 for proximal and 31.8 ± 2.9 stimuli for distal synapses). The decay in EPSC amplitudes from both proximal and distal synapses reached a plateau at 40–50 stimuli (Fig. 7*A* and *B*). Therefore, it appears that both proximal and distal synapses have a similarly large (Liu & Tsien, 1995; Stevens & Tsujimoto, 1995; Rosenmund & Stevens, 1996; Dobrunz & Stevens, 1997; Hagler & Goda, 2001) readily releasable pool of vesicles.

To examine further the possibility of an increase in synaptic size, we next compared the P_r between proximal and distal Schaffer collateral synapses. As the rate of antagonism by MK801 has been shown to be directly related to the P_r at hippocampal synapses, the impact of MK801 on trains of evoked NMDA EPSCs was compared between the synaptic populations (Hessler *et al.* 1993; Rosenmund *et al.* 1993).

NMDA EPSCs were evoked every 10 s with a bipolar stimulating electrode located ~20 μm adjacent to the recording electrode, and approximately 20 stable EPSCs were recorded prior to bath application of MK801 (5 μM). Electrical stimulation was terminated and MK801 was

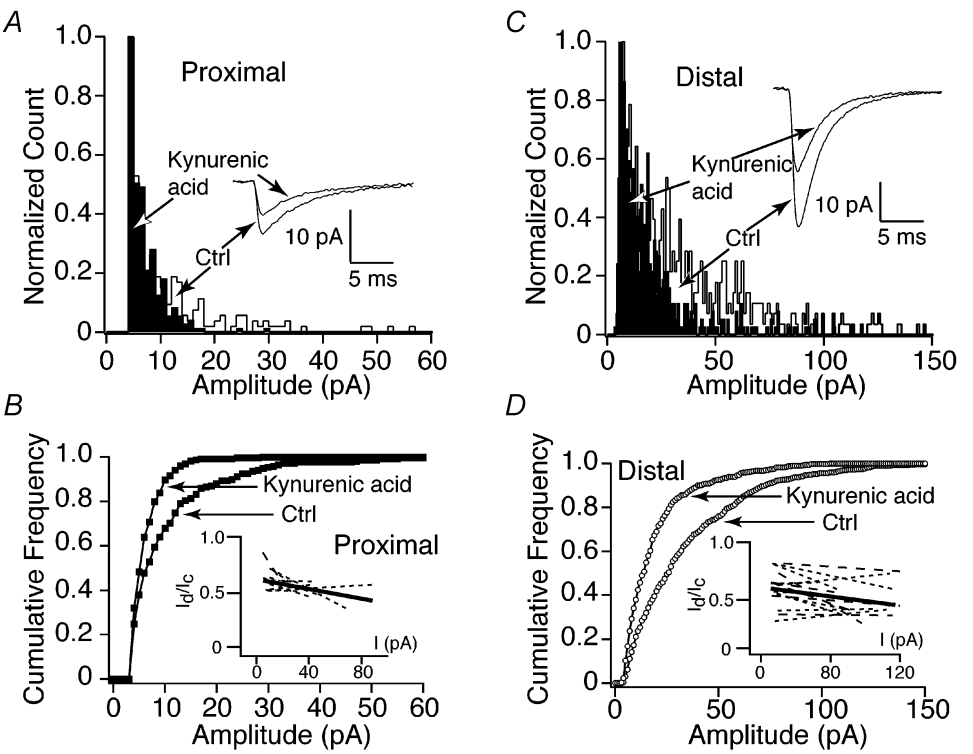

Figure 5. Kynurenic acid antagonizes mEPSCs equally in proximal and distal synapses

Normalized frequency histograms of osmolarity-evoked mEPSC amplitudes are shown for proximal (*A*) and distal synapses (*C*) in the absence and presence of kynurenic acid (200 μM, as indicated). The insets in *A* and *C* are representative ensembles of mean mEPSC traces in the presence and absence of kynurenic acid for proximal and distal synapses, respectively. Cumulative frequency distributions of mEPSC amplitudes are shown for proximal (*B*) and distal synapses (*D*) in the absence and presence of kynurenic acid (as indicated). The insets in *B* and *D* are plots of control (Ctrl) mEPSC amplitudes (I_c) against the ratio of mEPSC amplitudes in the presence and absence of kynurenic acid (I_d/I_c) at the same point on the cumulative frequency distribution. The dashed lines are linear regression plots from individual cells, whereas the continuous lines are the mean regressions of 10 and 15 cells for proximal and distal locations, respectively.

applied for 10 min. Following this, electrical stimulation was resumed and NMDA EPSC peak amplitude evoked by the first stimulus following MK801 incubation was reduced from control by 51 ± 9 % ($n = 6$) and 50 ± 2 % ($n = 6$) for proximal and distal regions, respectively (Fig. 8*A*). Furthermore, NMDA EPSC peak amplitudes progressively decreased in size with repeated stimulation in a double exponential function. The first and second decay time constants were 2.3 ± 0.9 and 24.8 ± 6.7 stimuli for proximal and 1.7 ± 0.4 and 28.4 ± 8.9 stimuli for distal synapses. The amplitude ratio of the fast and slow decay time constants was approximately 1:1 both in proximal and distal synapses. The fact that these time constants were not different between locations ($P > 0.4$) indicates that the probability of release was similar for both populations of synapses.

The magnitude of paired-pulse facilitation has long been related to P_r (Manabe *et al.* 1993; Debanne *et al.* 1996). We therefore examined the magnitude and time course of paired-pulse facilitation at proximal and distal synapses. Using a protocol that randomly altered the interval duration between the paired pulses (between 25 and 800 ms), 75–150 events per paired-pulse interval duration were collected at 0.1 Hz. As shown in Fig. 8*B*, the facilitation ratio ($\text{meanEPSC}_{(2nd)} - \text{meanEPSC}_{(1st)}/\text{meanEPSC}_{(1st)}$) for proximal synapses decays with a single exponential function of 108.8 ± 36.8 ms from a ratio of 1.57 ± 0.60 at a 25 ms interval duration to 0.1 ± 0.07 ($n = 6$) at a 800 ms interval duration. This effect of facilitation was mirrored at distal synapses, which decayed with a single exponential time constant of 165.5 ± 52.9 ms from a facilitation ratio of 1.82 ± 0.37 at the 25 ms interval to 0.08 ± 0.03 ($n = 6$) at the 800 ms interval. Therefore, the magnitude and time course of paired-pulse facilitation was comparable between the two populations of synapses, suggesting again that P_r was comparable. Hence, the data presented above suggest that the cleft glutamate concentration, the immediately releasable pool size and P_r do not differ among proximal and distal Schaffer collateral synapses, suggesting further that there are no location-dependent differences in synapse size.

Recent data from dendritic outside-out patches (Andrásfalvy & Magee, 2001) and single-photon glutamate uncaging experiments (Pettit & Augustine, 2000) have suggested that the density of AMPA channels is higher in distal dendritic regions. However, due to uncertainties as to the origin of patch receptors (i.e. synaptic or extrasynaptic) and the numbers of dendritic spines exposed to traditional glutamate uncaging

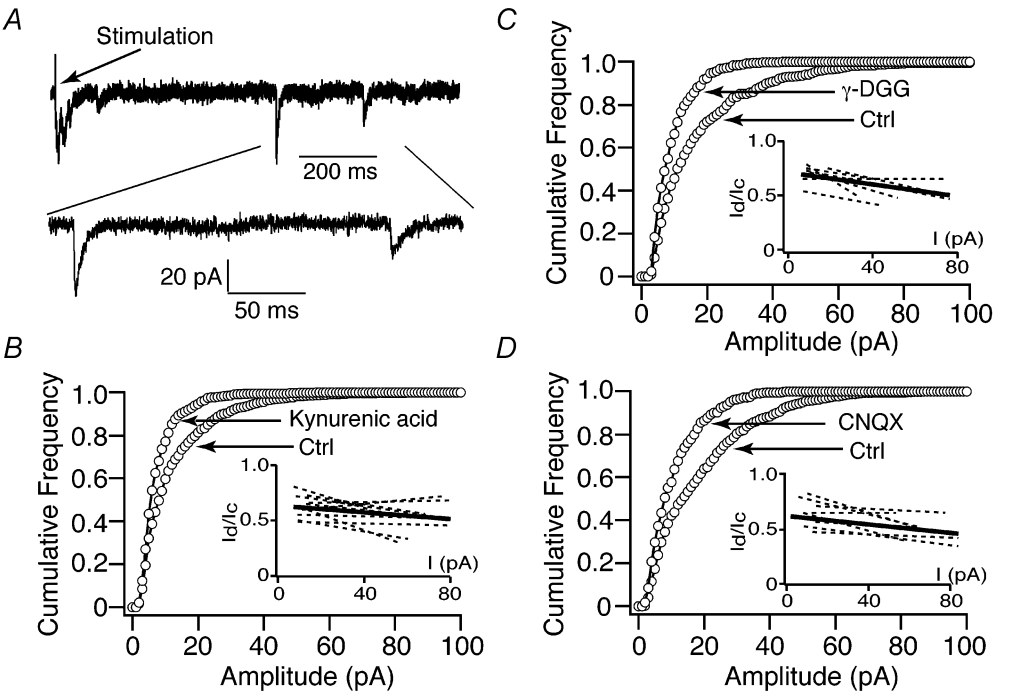

Figure 6. Fast and slow dissociating antagonists equally inhibit mEPSCs

A, localized electrical stimulation (where indicated) in the presence of 8 mM external Sr^{2+} desynchronizes multiple quantal events into single unitary events, as shown on the expanded time scale (bottom trace). Normalized cumulative frequency distributions of mEPSCs recorded and evoked at distal regions are shown in the absence or presence of kynurenic acid (200 μM; *B*), γ-D-glutamylglycine (γ-DGG, 1 mM; *C*) or 6-cyano-7-nitroquinoxaline-2,3-dione (CNQX, 500 nM; *D*). The insets in *B*, *C* and *D* are plots of control mEPSC amplitude (I_c) *versus* the ratio of mEPSC amplitudes in the presence and absence of antagonist (I_d/I_c) at same cumulative frequencies. The dashed lines are linear regression plots from individual cells, whereas the continuous lines are the mean regressions in the presence of kynurenic acid ($n = 10$), γ-DGG ($n = 9$) and CNQX ($n = 9$).

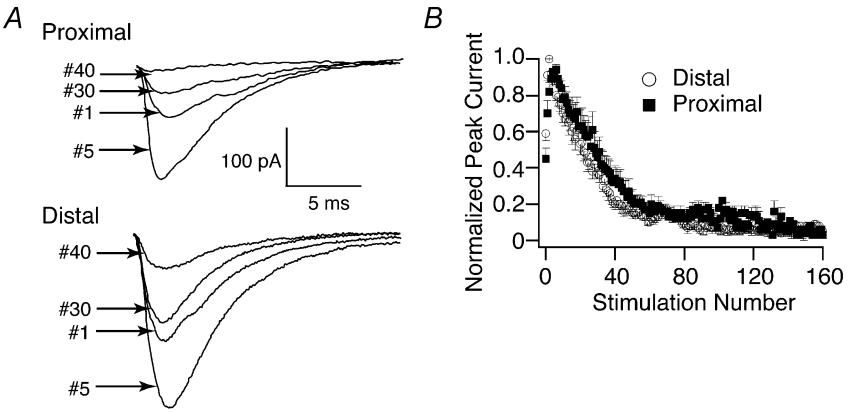

Figure 7. Immediately releasable vesicular pool sizes are the same at proximal and distal synapses

AMPA-mediated EPSCs were evoked with a bipolar stimulating electrode located at proximal and distal recording locations. Trains of electrical stimuli were delivered at 20 Hz in the presence of external 4 mM Ca^{2+}, 100 μM 4-aminopyridine and 2 μM 1,3-dipropyl-8-cyclopentylxanthine (DPCPX, an A1 receptor antagonist). *A*, representative current traces at different stimulation numbers within a stimulation train (indicated to the right of the traces) for proximal (~120 μm, top) and distal (~280 μm, bottom) EPSCs. *B*, stimulation number against normalized peak amplitude is shown for proximal (■) and distal (○) synapses. Each point is the mean ± S.E.M. for proximal ($n = 7$) and distal ($n = 5$) synapses.

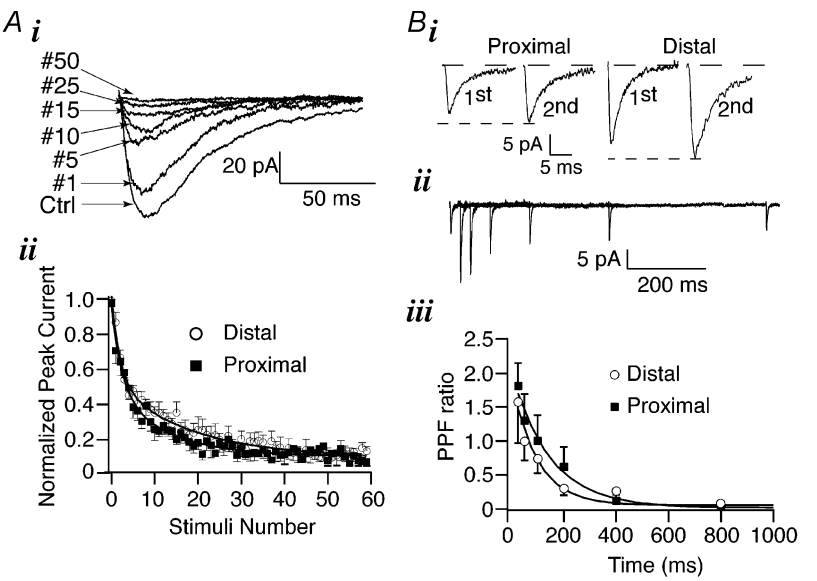

Figure 8. Proximal and distal synapses have similar release probabilities

A, electrically evoked NMDA EPSCs were stimulated every 10 s in the absence of external Mg^{2+} at proximal (■) and distal (○) recording locations. Sequences of ~20 stable amplitude EPSCs (Ctrl) were obtained prior to 10 min incubation with MK801 (5 μM) in the absence of electrical stimulation. *A*i, representative distal EPSC traces at different stimulation numbers (indicated to the left of the traces) following resumption of the stimuli in the presence of MK801. The stimulation number following MK801 incubation is shown in *A*ii plotted against normalized EPSC peak amplitude. Plots of progressive MK801 antagonism of NMDA EPSCs are fitted with double exponential functions ($n = 6$). *B*, minimal electrical stimulation intensities were delivered to proximal and distal recording sites by a bipolar stimulating electrode at 0.1 Hz. *B*i, representative mean AMPA mEPSC traces (i.e. excluding failures) are shown during pairs of stimulations separated by a 50 ms interval (1st and 2nd pulses) for proximal (left) and distal (right) locations. *B*ii, representative mean mEPSCs (including failures) are shown superimposed for the first pulse and at 25, 50, 100, 200, 400 and 800 ms paired-interval durations. *B*iii, interval duration against the paired-pulse facilitation (PPF; $\text{meanEPSC}_{(2nd)} - \text{meanEPSC}_{(1st)}/\text{meanEPSC}_{(1st)}$) ratio is shown for proximal (■) and distal (○) events ($n = 6$).

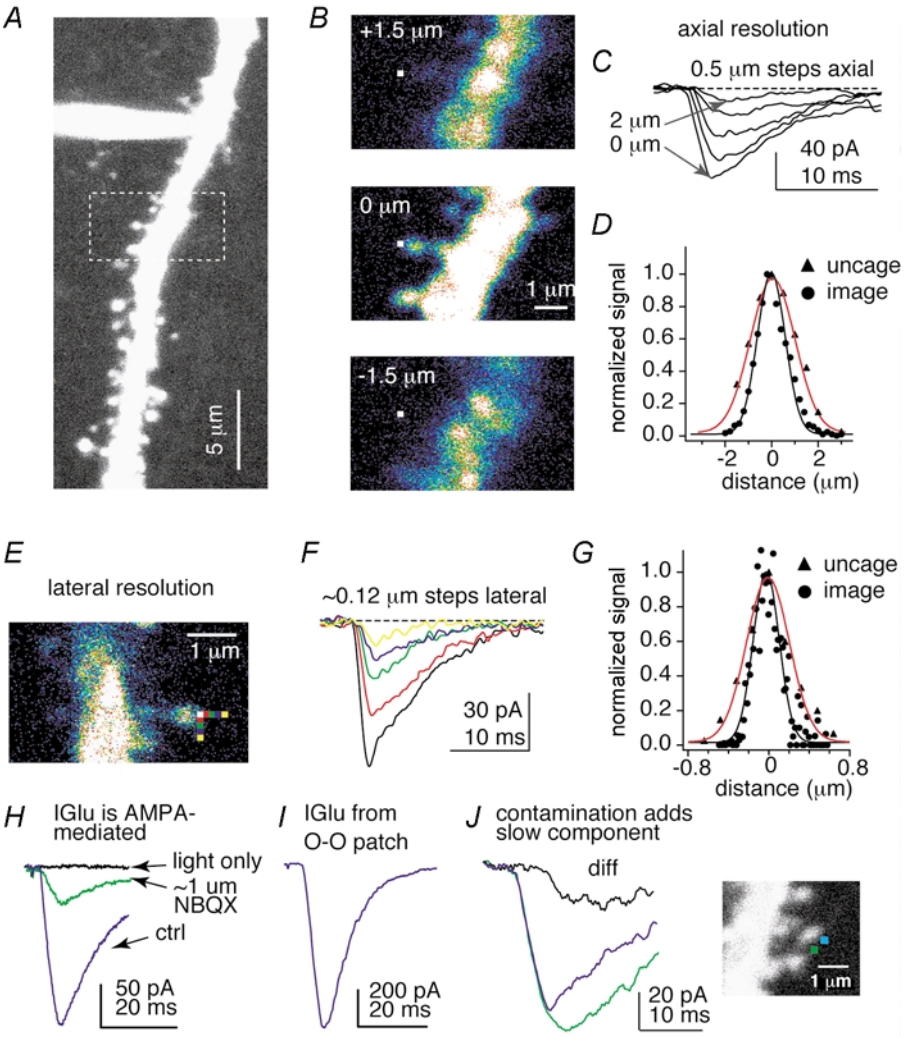

Figure 9. Spatial resolution and properties of MNI-glu currents

A, image stack of a distal apical dendritic trunk (pipette at ~275 μm). *B*, single sections of area bound by dashed box in *A*). The middle image is the primary uncaging section, while the upper and lower images are 1.5 μm above and below that section, respectively. Note that there are no other spines within 1 μm lateral of the recorded spine on any axial plane. *C*, MNI-glu currents (I_{Glu}) evoked (5 mW, 720 nm, 2 ms) at different axial locations from spine shown in *B*). Each current is an average of two currents evoked ± Δx from the original uncaging section (0 μm). *D*, plots of imaging and uncaging lateral resolution (see below). *E*, single section of another spine from a different cell. Coloured squares show uncaging locations that correspond with evoked current traces shown at the right (*F*). Each current is an average of one current evoked at each of the two lateral locations shown (current at the white location was evoked twice). *G*, plots of imaging and uncaging axial resolution. Imaging curves are fluorescence profiles for 0.1 μm fluorescent beads (circles, normalized to maximum fluorescence), while uncaging curves are plots of MNI-glu-evoked current amplitude (triangles, normalized to maximum current). Continuous lines are fits of the data by Gaussian functions with resolutions determined from the full width, half maximum (imaging: 0.34 μm lateral and 1.44 μm axial; uncaging: 0.6 μm lateral, 2.0 μm axial). *H*, MNI-glu currents were inhibited by 1,2,3,4-tetrahydro-6-nitro-2,3-dioxo-benzo[f]quinoxaline-7-sulphonamide (NBQX; the final concentration is unknown as 5 μM NBQX was bath-applied while MNI-glu was delivered simultaneously via a puffer pipette that contained no NBQX). No current was evoked by light alone (black trace). *I*, currents could be evoked by uncaging glutamate onto dendritic outside-out patches, demonstrating that only the postsynaptic membrane is required. *J*, when a spine was isolated, evoked currents exhibited monotonic rise kinetics. Moving the uncaging location to a spot that is closer to another spine (from the blue to the green square) resulted in the presence of an additional slow component in the rise phase that is presumably due to diffusion onto the second spine. Only MNI-glu currents showing a monotonic rise phase were analysed.

methods, we chose to re-examine this issue. Multiphoton irradiation was used to focally uncage glutamate onto single isolated dendritic spines *in situ*, as described previously (Matsuzaki *et al.* 2001).

Neurons were filled with bis-Fura2 (150 μM) and all recorded dendrites were within 15–20 μm of the slice surface. MNI-glu (~12 mM) was applied via a broken patch pipette that was positioned on the surface of the slice at the dendritic region in the immediate vicinity of the recording pipette. Mode-locked laser light (720 nm) of different intensities was used for imaging of the dendrite (2 mW) as well as uncaging MNI-glu (5 mW). Once a well-isolated spine was found near the recording pipette (see Methods and Fig. 9), 2–4 ms pulses of light were given to release glutamate and the uncaging location was moved in ~0.12 μm steps around each spine head under study in order to locate the maximum current response of each spine. The spot producing the largest amplitude was used as the measure of spine current and presumably correlates with the location of the postsynaptic density (PSD). Recordings from GluR1−/− mice, which lack any significant extrasynaptic AMPA receptor population, suggest that the vast majority of receptors activated by this glutamate uncaging procedure are of synaptic origin (authors' unpublished observation).

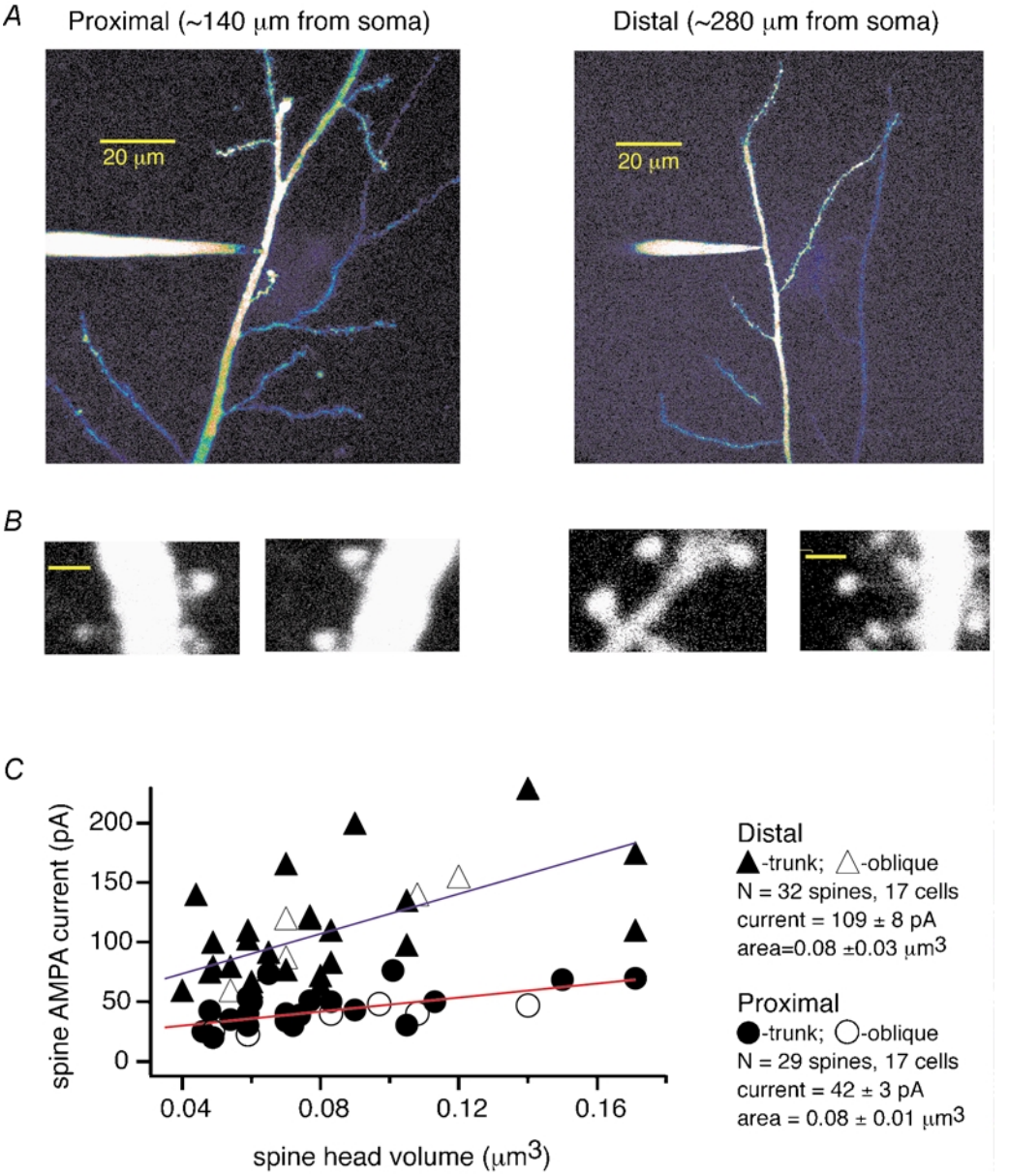

Figure 10. Distal spines show an increased AMPA receptor current

A, examples of proximal and distal recording configurations. *B*, examples of isolated spines from which MNI-glu currents were evoked. Scale bar = 1 μm. *C*, plot of MNI-glu spine AMPA current amplitude for proximal and distal spines *versus* area of the spine head. Note that the slope of the relationship increases with distance (slope = 128 *versus* 327 pA μm^{-3}, proximal *versus* distal).

In agreement with Matsuzaki *et al.* (2001), a positive correlation existed between spine head volume and evoked currents in all regions studied, with larger spines producing larger currents (slope = 128 *vs.* 327 pA μm^{-3}, proximal *versus* distal; Fig. 10). Although the mean volume of the spines examined at proximal and distal regions were the same (proximal 0.08 ± 0.01 μm^3, 29 spines, $n = 17$; distal 0.08 ± 0.03 μm^3, 32 spines, $n = 17$), the current amplitudes obtained from the different locations were significantly different. The mean AMPA-receptor-mediated current obtained from proximal trunk and nearby oblique synapses was 42 ± 3 pA, which contrasted

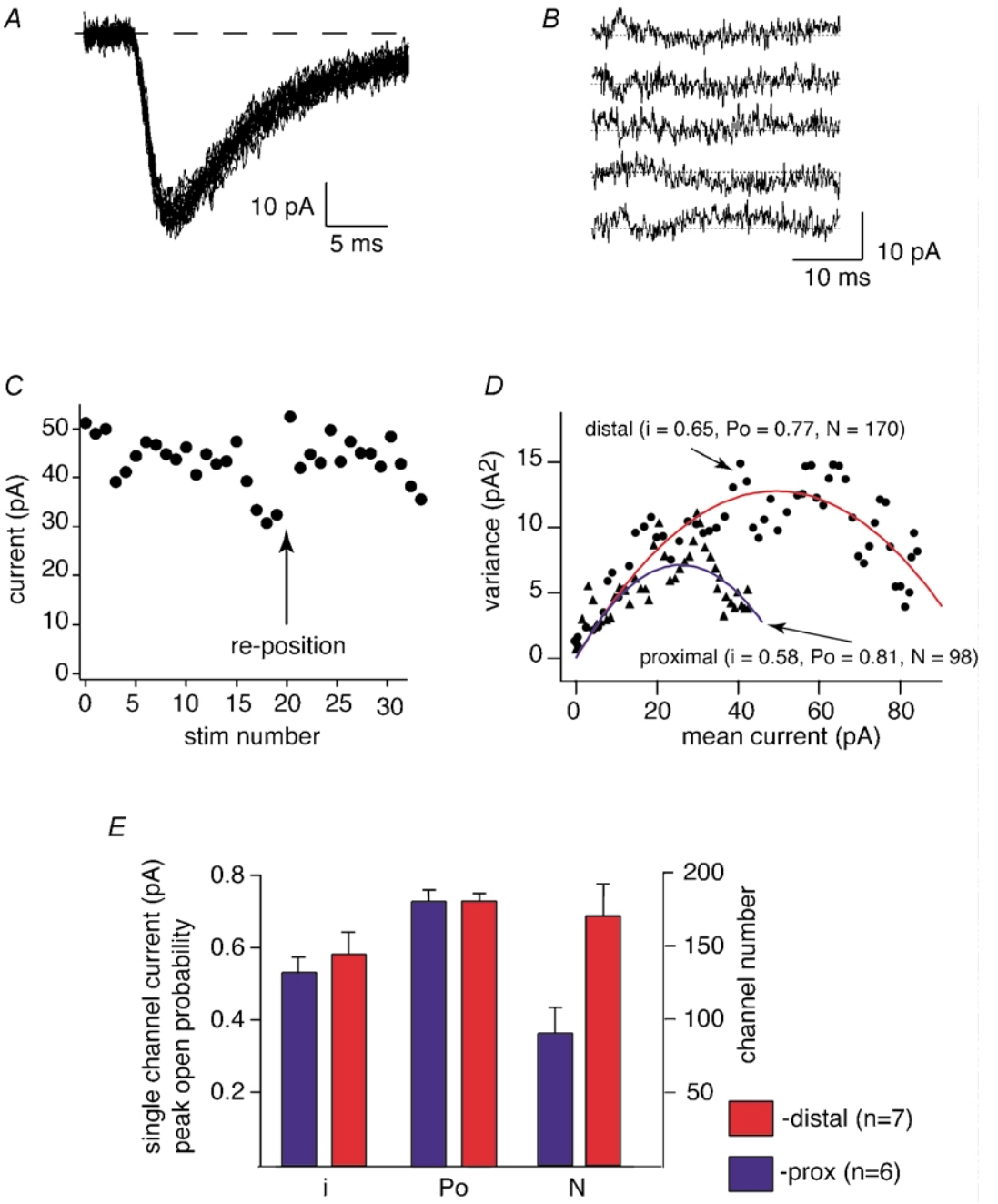

Figure 11. Non-stationary fluctuation analysis (NSFA) of AMPA currents

A, representative MNI-glu currents used in NSFA of the proximal spine currents shown in *D*. *B*, representative difference currents (individual − mean) from the same spine. *C*, plot of consecutive current amplitude for currents shown in *A*. Note that the uncaging location was reset at the time indicated by the arrow due to some movement of the spine/slice. *D*, plot of mean current *versus* variance for 29–40 sequentially evoked currents from representative proximal (▲) and distal (●) spines. Data were fitted by parabolic functions (proximal blue line, distal red line). Raw variance points were binned at 0.5 pA. *E*, grouped data from NSFA showing near doubling of distal AMPA-receptor numbers, while single-channel current and open probability remained constant.

with 109 ± 8 pA obtained from proximal trunk and nearby oblique synapses. These synapse-level differences may suggest that distal dendritic spines have a higher density of AMPA receptors. To confirm that the increase in AMPA current evoked at distal spines was not due to higher channel P_o or unitary conductance, non-stationary fluctuation analysis was performed (Fig. 11). Data for noise analysis was gained by repeated uncaging of MNI-glu onto isolated spines of similar size (proximal 0.06 ± 0.01 μm^3, distal 0.07 ± 0.01 μm, $P > 0.3$) in stable sequences. Mean current from multiple trials (initial 10–25 ms) was plotted against the variance of each trial and fitted with a parabolic function (see Methods). Although single-channel current (proximal 0.5 ± 0.04 pA, $n = 6$; distal 0.6 ± 0.06 pA, $n = 7$) and P_o (proximal 0.77 ± 0.03, distal 0.78 ± 0.02) did not differ spatially, the number of channels on distal spines was approximately twofold greater than proximal spines (proximal 91 ± 17, distal 171 ± 21, $P < 0.01$). These data thus confirm that distance-dependent scaling of AMPA-receptor-mediated synaptic conductance is due to an increase in postsynaptic receptor density.

DISCUSSION

Data presented in this study demonstrate that the rise and decay time constants (in the absence of desensitization) of proximal and distal mEPSCs are positively correlated with amplitude. This observation is consistent with a Monte Carlo model that shows that increasing the concentration of glutamate released in the absence of receptor desensitization, generates mEPSCs that are larger in amplitude and have slower rise and decay time constants (Glavinovic & Rabie, 1998). However, plots of normalized mEPSC amplitude *versus* rise or decay time constants revealed no significant differences between proximal and distal events. This may indicate that proximal synapses experience the same range of cleft glutamate concentrations as distal synapses. The location-independent effect of rapid-off competitive antagonists seems to substantiate this idea.

The number of vesicles docked at the active zone, the size of the active zone and the P_r all co-vary with the postsynaptic density area and transmitter receptor number (Takumi *et al.* 1999). Along these lines, recent evidence suggests that the number of AMPA receptors present at distal dendritic sites is greater than at more proximal locations (Andrásfavly & Magee, 2001). Thus it seems possible that the average size of the Schaffer collateral synapse could increase with distance from the soma. In fact, similar changes have already been observed in other central neurons (Triller *et al.* 1990; Sur *et al.* 1995; Alvarez *et al.* 1997). If this was indeed the case, we would expect that the immediately releasable pool size, the P_r and paired-pulse facilitation magnitudes would be dependent on synapse location. The fact that this was not observed is strong evidence that the range and the mean synapse size does not increase with distance. Indeed, a recent anatomical study would seem to confirm this conclusion (Megías *et al.* 2001).

As mean synaptic size does not appear to increase with distance, the increase in the number of AMPA receptors in distal outside-out patches is likely to be due to an increase in the density of AMPA receptors at distant synapses. That larger AMPA-receptor-mediated currents were evoked at distal spines would seem to confirm this hypothesis. Non-stationary fluctuation analyses indicate further that the increase in AMPA-receptor-mediated current is not due to differences in single-channel conductance or P_o, but instead to a larger number of AMPA receptors per spine. These data can be interpreted in two ways: first, that the AMPA-receptor density in the PSD is progressively increased with distance, or second, that AMPA-receptor density is maintained while instead the size of the PSD increases with distance from the soma. In this case, the relationship between spine volume and PSD area would be changed, and there is some limited data suggesting that such a situation does not occur in Schaffer collateral synapses (Megías *et al.* 2001).

In conclusion, Schaffer collateral axons form what appears to be a single functional population of excitatory synapses within the stratum radiatum of hippocampal area CA1. While the fundamental properties of individual synapses can vary greatly from one to another, the postsynaptic neuron has undergone several major modifications that, under certain conditions, allow the impact of these synapses to be independent of their dendritic location (Magee, 2000). The ability of Schaffer collateral synapses to function in a location-independent manner increases the computational repertoire of CA1 pyramidal neurons, and has important implications for the use of associative synaptic plasticity for information storage in these cells. The main question remaining is, what mechanisms are capable of preferentially increasing the number of AMPA receptors on distal dendritic spines? Recent work investigating the role of postsynaptic AMPA receptor cycling in activity-dependent synaptic scaling (Turrigiano & Nelson, 2000) as well as certain forms of long-term synaptic plasticity (Malinow & Malenka, 2002) appear to provide some direction for future experiments.

REFERENCES

Alvarez FJ, Dewey DE, Harrington DA & Fyffe RE (1997). Cell-type specific organization of glycine receptor clusters in the mammalian spinal cord. *J Comp Neurology* **379**, 50–70.

Andrásfalvy BK & Magee JC (2001). Distance-dependent increase in AMPA receptor number in the dendrites of adult hippocampal CA1 pyramidal neurons. *J Neurosci* **21**, 9151–9159.

Bekkers JM & Clements JD (1999). Quantal amplitude and quantal variance of strontium-induced asynchronous EPSCs in rat dentate granule neurons. *J Physiol* **516**, 227–248.

Choi S, Klingauf J & Tsien RW (2000). Postfusional regulation of cleft glutamate concentration during LTP at 'silent synapses'. *Nat Neurosci* **3**, 330–336.

Clements JD, Lester RA, Tong G, Jahr CE & Westbrook GL (1992). The time course of glutamate in the synaptic cleft. *Science* **258**, 1498–1501.

Debanne D, Guerineau NC, Gähwiler BH & Thompson SM (1996). Paired-pulse facilitation and depression at unitary synapses in rat hippocampus: quantal fluctuation affects subsequent release. *J Physiol* **491**, 163–176.

Diamond JS & Jahr CE (1995). Asynchronous release of synaptic vesicles determines the time course of the AMPA receptor-mediated EPSC. *Neuron* **15**, 1097–1107.

Dobrunz LE & Stevens CF (1997). Heterogeneity of release probability, facilitation, and depletion at central synapses. *Neuron* **18**, 995–1008.

Glavinovic MI & Rabie HR (1998). Monte Carlo simulation of spontaneous miniature excitatory postsynaptic currents in rat hippocampal synapse in the presence and absence of desensitization. *Pflugers Arch* **435**, 193–202.

Hagler DJ Jr & Goda Y (2001). Properties of synchronous and asynchronous release during pulse train depression in cultured hippocampal neurons. *J Neurophysiol* **85**, 2324–2334.

Hessler NA, Shirke AM & Malinow R (1993). The probability of transmitter release at a mammalian central synapse. *Nature* **366**, 569–572.

Inasek R & Redman SJ (1973). The amplitude, time course and charge of unitary excitatory post-synaptic potentials evoked in spinal motorneurone dendrites. *J Physiol* **234**, 665–688.

Jack JJ & Redman SJ (1971). The propagation of transient potentials in some linear cable structures. *J Physiol* **215**, 283–320.

Jaffe DB & Carnevale NT (1999). Passive normalization of synaptic integration influenced by dendritic architecture. *J Neurophysiol* **82**, 3268–3285.

Korn H, Bausela F, Carpier S & Faber DS (1993). Synaptic noise and multiquantal release at dendritic synapses. *J Neurophysiol* **70**, 1249–1253.

Liu G, Choi S & Tsien RW (1999). Variability of neurotransmitter concentration and nonsaturation of postsynaptic AMPA receptors at synapses in hippocampal cultures and slices. *Neuron* **22**, 395–409.

Liu G & Tsien RW (1995). Properties of synaptic transmission at single hippocampal synaptic boutons. *Nature* **375**, 404–408.

Magee J (1998). Dendritic hyperpolarization-activated currents modify the integrative properties of hippocampal CA1 pyramidal neurons. *J Neurosci* **18**, 7613–7624.

Magee JC (2000). Dendritic integration of excitation synaptic input. *Nat Rev Neurosci* **1**, 181–190.

Magee JC & Cook EP (2000). Somatic EPSP amplitude is independent of synapse location in hippocampal pyramidal neurons. *Nat Neurosci* **3**, 895–903.

Malinow R & Malenka RC (2002). AMPA receptor trafficking and synaptic plasticity. *Annu Rev Neurosci* **25**, 103–126.

Manabe T, Wyllie DJ, Perkel DJ & Nicoll RA (1993). Modulation of synaptic transmission and long-term potentiation: effects on paired pulse facilitation and EPSC variance in the CA1 region of the hippocampus. *J Neurophysiol* **70**, 1451–1459.

Matsuzaki M, Ellis-Davies GCR, Nemoto T, Miyashita Y, Iino M & Kasai H (2001). Dendritic spine geometry is critical for AMPA receptor expression in hippocampal CA1 pyramidal neurons. *Nat Neurosci* **4**, 1086–1092.

Megías M, Emre ZS, Freund TF & Gulyas AI (2001). Total number and distribution of inhibitory and excitatory synapses on hippocampal CA1 pyramidal cells. *Neuroscience* **102**, 527–540.

Pettit DL & Augustine GJ (2000). Distribution of functional glutamate and GABA receptors on hippocampal pyramidal cells and interneurons. *J Neurophysiol* **84**, 28–38.

Rall W (1962). Theory of physiological properties of dendrites. *Ann N Y Acad Sci* **96**, 1071–1079.

Rall W (1967). Distinguishing theoretical synaptic potentials computed for different soma-dendritic distributions of synaptic input. *J Neurophysiol* **30**, 1138–1168.

Rammes G, Swandulla D, Spielmanns P & Parsons CG (1998). Interactions of GYKI 52466 and NBQX with cyclothiazide at AMPA receptors: experiments with outside-out patches and EPSCs in hippocampal neurones. *Neuropharmacology* **37**, 1299–1320.

Rosenmund C, Clements JD & Westbrook GL (1993). Nonuniform probability of glutamate release at a hippocampal synapse. *Science* **262**, 754–757.

Rosenmund C & Stevens CF (1996). Definition of the readily releasable pool of vesicles at hippocampal synapses. *Neuron* **16**, 1197–1207.

Schikorski T & Stevens CF (1999). Quantitative fine structure analysis of olfactory cortical synapses. *Proc Nat Acad Sci U S A* **96**, 4107–4112.

Schikorski T & Stevens CF (2001). Morphological correlates of functionally defined synaptic vesicle populations. *Nat Neurosci* **4**, 391–395.

Sigworth FJ (1980). The variance of sodium current fluctuations at the node of Ranvier. *J Physiol* **307**, 97–129.

Stevens CF & Tsujimoto T (1995). Estimates for the pool size of releasable quanta at a single central synapse and for the time required to refill the pool. *Proc Natl Acad Sci U S A* **92**, 846–849.

Stricker C, Fiel AC & Redman SJ (1996). Statistic analysis of amplitude fluctuations in EPSCs evoked in rat CA1 pyramidal neurones *in vitro*. *J Physiol* **490**, 419–441.

Sur C, Triller A & Korn H (1995). Morphology of the release site of inhibitory synapses on the soma and dendrite of an identified neuron. *J Comp Neurol* **351**, 247–260.

Takumi Y, Ramirez-Leon V, Laake P, Rinvik E & Ottersen OP (1999). Different modes of expression of AMPA and NMDA receptors in hippocampal synapses. *Nat Neurosci* **2**, 618–624.

Triller A, Seitanidou T, Franksson O & Korn H (1990). Size and shape of glycine receptor clusters in a central neuron exhibit a somato-dendritic gradient. *New Biol* **2**, 637–641.

Trussell LO, Zhang S & Raman IM (1993). Desensitization of AMPA receptors upon multiquantal release. *Neuron* **10**, 1185–1196.

Turrigiano GG & Nelson SB (2000). Hebb and homeostasis in neuronal plasticity. *Curr Opin Neurobiol* **10**, 358–364.

Vyklicky L Jr, Patneau DK & Mayer ML (1991). Modulation of excitatory synaptic transmission by drugs that reduce desensitization at AMPA/kainate receptors. *Neuron* **7**, 971–984.

Williams SR & Stuart GJ (2002). Dependence of EPSP efficacy on synapse location in neocortical pyramidal neurons. *Science* **295**, 1907–1910.

Acknowledgements

This work was supported by National Institutes of Health grants NS 35865, NS 39458 to JCM and GM53395, NSF 0090826 and the McKnight Endowment Fund to GED.